

Tuning the interplay of spin-orbit coupling and trigonal crystal-field effect in the Ising-like spin system $\text{Ca}_3\text{Co}_2\text{O}_6$

Santanu De¹,² Amit Chauhan,^{2,3,4} B. R. K. Nanda,^{2,3,4} and A. Banerjee¹

¹UGC-DAE Consortium for Scientific Research, University Campus, Khandwa Road, Indore 452001, India

²Condensed Matter Theory and Computational Lab, Department of Physics, IIT Madras, Chennai 600036, India

³Center for Atomistic Modelling and Materials Design, Indian Institute of Technology Madras, Chennai 600036, India

⁴Functional Oxide Research Group, Indian Institute of Technology Madras, Chennai 600036, India



(Received 4 March 2022; revised 17 November 2022; accepted 4 January 2023; published 24 January 2023)

In the $\text{Ca}_3\text{Co}_2\text{O}_6$ (CCO) system, the large contribution of the orbital moment to the magnetization and the strong magnetocrystalline anisotropy (MCA) are considered to give rise to the Ising magnetism. In this study, the dominant role of both spin-orbit-coupling (SOC) and crystal-field (CF) effects behind this Ising character of magnetism is qualitatively elucidated from the temperature and field dependence of magnetization in the presence of hydrostatic pressures up to 1.04 GPa in a CCO single crystal (SC). The local trigonal prismatic environment is compressed with the application of high pressure, resulting in higher trigonal CF as compared to ambient conditions. It reduces the effect of SOC due to the initiation of orbital quenching that finally decreases orbital moment contributions to both the magnetization and the MCA, respectively. This interplay of trigonal CF and SOC effects is further shown from the detailed quantitative analysis of the field-dependent magnetization in different orientations of CCO and $\text{Ca}_3\text{Co}_{1.8}\text{Fe}_{0.2}\text{O}_6$ (CCFO) SCs at ambient pressure by employing a simple classical model and second-order perturbative analysis of SOC. The complete quenching of the orbital moment of Fe^{3+} ($S = 5/2$) in CCFO weakens the MCA and also helps in deducing the SOC effect. Furthermore, the estimated anisotropic constants using density functional theory very well capture the Ising magnetism in CCO and deviation from it in CCFO compared to that of classical results.

DOI: [10.1103/PhysRevB.107.014418](https://doi.org/10.1103/PhysRevB.107.014418)

I. INTRODUCTION

Strong spin-orbit-coupling (SOC)-induced Ising magnetism has drawn huge attention in recent years and it has been investigated in a great variety of magnetic systems [1–16]. The spin chain compound $\text{Ca}_3\text{Co}_2\text{O}_6$ (CCO) is one of the important candidates belonging to this class of material due to its fascinating magnetic properties [8–31]. It is crystallized in a rhombohedral structure where the spin chain of Co_2O_6 is formed by the alternating arrangement of nonmagnetic octahedra (OCT) ($S = 0$) and magnetic trigonal prism (TP) ($S = 2$) sites under the space group $R\bar{3}c$ [11,15,17–21]. It has been established that different values of the residual crystalline field along the chain promotes two distinct spin states of Co^{3+} ions at two consecutive sites. The behavior of this spin chain compound has been considered as a one-dimensional system at high temperature due to one order higher magnitude of the ferromagnetic (FM) intrachain interaction strength among $S = 2$ Co^{3+} ions as compared to the average interchain coupling [18,22–25]. However, this spin system is ordered in a three-dimensional (3D) ferrimagnetic (FIM) state at low temperature due to the influence of both intrachain and interchain couplings [14,26–31]. In a high magnetic field, this 3D FIM state converts to 3D FM state [14,17–19,26–31].

Moreover, the presence of an unconventional orbital magnetic moment in the magnetization and the magnetocrystalline anisotropy (MCA) are the two important aspects to reconcile

the Ising-like behavior of this spin chain system. An enormous theoretical and experimental effort has been devoted to understanding this issue. Initially, the magnetic anisotropy of the FM chain has been described by Kageyama *et al.* in a magnetization study in random and aligned (along the c axis) powders of the CCO system [9]. A random or partially ordered system might introduce a considerable amount of error in the anisotropy estimation. Later on, the anisotropic nature of the magnetic susceptibility in CCO single crystals (SC) has been established by Hardy *et al.* and the reported data were presented down to 50 K in this study [10]. Moreover, the existence of both the crystal-field effect and SOC has been argued in the CCO spin system from density functional theory calculation. It gives rise to a large orbital moment contribution to the magnetization and strong MCA, respectively [11,12]. However, the crystal-field splitting of the cobalt d orbital is one of the debated issues in these studies [11,12]. The orbital contribution is also confirmed by the observed saturation moment ($\sim 5.0 \mu_B$) in magnetization studies and the extracted value of the large orbital moment ($\sim 1.7 \mu_B$) from the analysis of x-ray magnetic circular dichroism (XMCD) [13–15,30]. Thus, both the SOC and the trigonal crystal-field effects have a significant role in the Ising-like character of the CCO spin system. On the contrary, a non-Ising-like behavior has been reported by Cheng *et al.* that might result from the helical exchange pathways in this spin system [16]. These controversies

have led us to further explore the nature of magnetism in this prototype spin chain system.

To shed light on this, an attempt is made here by controlling orbital degrees of freedom through oxygen-ligand field modulation at the TP site. This is achieved here by applied external high pressure and chemical substitution of Fe^{3+} ($S = 5/2$), respectively, in the CCO spin system. Strengthening of the trigonal CF effect with the application of hydrostatic pressure reduces the domination of SOC due to the higher tendency of orbital quenching at high pressure with respect to ambient conditions in CCO SC. It reduces both the orbital moment contribution to magnetization and the MCA. At the same time, the exactly half-filled d shell of Fe^{3+} ($S = 5/2$) quenches the orbital moment of iron in $\text{Ca}_3\text{Co}_{1.8}\text{Fe}_{0.2}\text{O}_6$ (CCFO) SC. As a result, effective SOC has been reduced in CCFO SC as compared to CCO, resulting in the decrease of the MCA. Here, it is clearly shown that both SOC and CF effects are playing crucial roles in the orbital moment contributions to the magnetization and the MCA which are ultimately responsible for the Ising nature of magnetism in the CCO system.

II. EXPERIMENTAL DETAILS

Single crystals of $\text{Ca}_3\text{Co}_2\text{O}_6$ and $\text{Ca}_3\text{Co}_{1.8}\text{Fe}_{0.2}\text{O}_6$ were grown with the flux method using K_2CO_3 flux [14]. The needle shape crystals had a length of ~ 3 mm along the c axis. The field and temperature dependencies of magnetization along the c axis of CCO single crystals were carried out at various hydrostatic pressures with a superconducting quantum interface device magnetometer (MPMS-3, Quantum Design, USA). Daphne-7373 oil was used as the pressure transmitting medium inside the copper-beryllium cell. A small piece of superconducting Sn wire was used to calibrate the high pressure. In this experiment, one of the main difficulties is the orientation fixing of a CCO single crystal. This was resolved by cooling the system in the presence of a 70-kOe field down to the freezing point of the Daphne-7373 oil, and thereafter, the cooling field was isothermally switched off. In this method, the crystallographic c axis of the CCO single crystal can easily be aligned parallel to the applied magnetic field as compared to the ab plane which is supported by the experimentally observed saturation moment. At the same time, magnetization measurements along different crystallographic axes of CCO and CCFO single crystals were performed at ambient pressure using the vibrating sample magnetometer (± 160 kOe, Quantum Design, USA).

III. RESULT AND DISCUSSIONS

A. High-pressure studies

Figure 1(a) shows the temperature dependence of magnetization at 5 kOe in the field-cooled mode along the c axis of a CCO single crystal at various hydrostatic pressures. It suggests that a three-dimensional ferrimagnetic state stabilizes below the onset point of long-range ordering ($T_{\text{LRO}} \sim 25$ K) at ambient pressure. This T_{LRO} shifts to higher temperature with the application of hydrostatic pressure as shown in the inset of Fig. 1(a). At the same time, the magnetization of the low- T 3D FIM state is found to decrease at higher pressure as compared to ambient conditions. Reduction of the magnetization of the

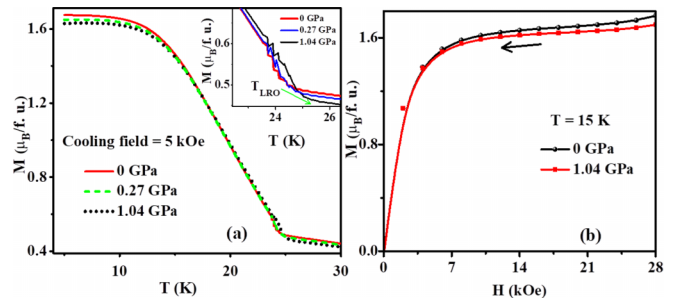


FIG. 1. (a) Variation of field-cooled magnetization as a function of temperature at 5 kOe, whereas the inset shows the zoomed-in view of $M(T)$ around long-range ordering. (b) Zoomed-in view of field-dependent magnetization in the low-field range at 15 K in two different hydrostatic pressures.

low- T 3D FIM state is further confirmed by field-dependent magnetization measurements along the c axis at 15 K in the field decreasing branch which is shown in Fig. 1(b). The zoomed-in view of the field dependence of magnetization in the lower field range is depicted in Fig. 1(b) for the sake of clarity. It clearly supports the lessening of the magnetization associated with the low- T 3D FIM state at higher pressures. Due to difficulties in fixing the single-crystal orientation inside the pressure cell the magnetization data were not recorded along the hard axis (ab plane).

Figure 2(a) represents the variation of magnetization as a function of the field along the crystallographic c axis at 15 K at two different applied pressures. Similar to earlier observations (see the Refs. [14,17,30,31]), magnetic field cycling converts the 3D ferrimagnetic state to a fully saturated 3D FM state with a saturation magnetization of $\sim 5.0 \mu_B$ for parallel orientation of the c axis of the CCO single crystal with respect to the field direction. Considering the high-spin state of trivalent Co at the TP site due to different residual crystal electric fields as compared to the OCT site along the chain in the CCO system, i.e., $S = 2$ (Co^{3+}), the spin-only moment would be at about $4.0 \mu_B$, whereas the experimentally observed saturation is at $\sim 5.0 \mu_B$. Thus, the remaining moment is thought to come from the orbital contribution. This is consistent with previous reports of magnetization, neutron diffraction, and XMCD studies in the CCO spin system [13–15,24,30]. There are many cobaltate systems, such as LaCoO_3 , $\alpha\text{-CoV}_2\text{O}_6$, and

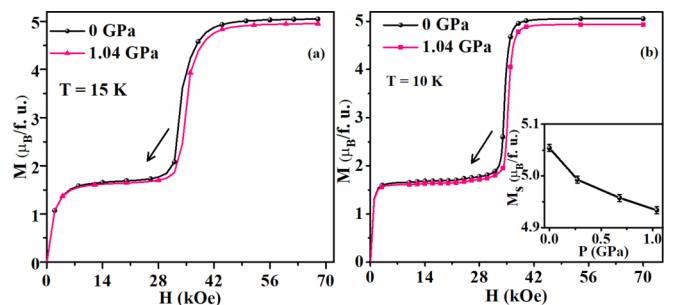


FIG. 2. Plot of magnetization as a function of field at different hydrostatic pressures at (a) 15 K and (b) 10 K, respectively. The inset of panel (b) illustrates the pressure dependence of the saturation magnetization at 10 K.

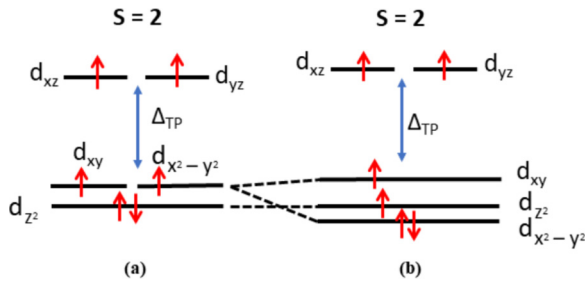


FIG. 3. Splitting of d orbitals of cobalt ions at the trigonal prism site due to (a) the crystal-field effect and (b) both crystal-field and SOC effects.

γ -CoV₂O₆, showing such a huge contribution of the orbital moment to the magnetization [2–4]. The presence of this large orbital contribution also indicates the existence of SOC in this spin system that leads to a strong MCA. This anisotropic nature of the magnetism behavior has already been established in this system [9–12,14,16]. Therefore, it is evident that the large contribution of the orbital moment to the magnetization and the strong MCA are the outcome of SOC and trigonal crystal-field effects in this system. Further, the saturation moment of the 3D FM state is decreased with the application of hydrostatic pressure (up to $P \sim 1.04$ GPa) like that of the 3D FIM state. Moreover, similar to 15 K, the reduction of the magnetization of both 3D FIM and 3D FM states is observed in the field dependence of the magnetization along the c axis at 10 K with increasingly higher pressure, which is demonstrated in Fig. 2(b). The inset of Fig. 2(b) depicts the variation of the saturation magnetization of the fully magnetized 3D FM state with applied pressures at 10 K. It shows that magnetization of the 3D FM state is reduced by 3% with applied pressure up to 1.04 GPa as compared to 0 GPa. This small change in the magnetization of both 3D FIM and 3D FM states with hydrostatic pressure might be entirely dominated by modulation of the orbital moment, because the substantial change in magnetization due to spin-crossover will be significantly high as observed in LaCoO₃ and many other systems [2,32–34].

To interpret this orbital modulation and its consequences, the splitting of fivefold degenerate atomic d orbitals of cobalt in the crystal environment of the CCO system has been discussed by considering the crystal-field and SOC effects, respectively. In the CCO compound, Co³⁺ (high spin) d orbitals at the TP site splits as $[d_{z^2} (d_{x^2-y^2} d_{xy}) (d_{xz} d_{yz})]$ due to the crystal-field effect which is depicted in Fig. 3(a) [12,35]. Inclusion of the spin-orbit interaction to this crystal-field splitting brings down the $d_{x^2-y^2}$ orbital and lifts the degeneracy of $(d_{x^2-y^2} d_{xy})$ states; this is schematically demonstrated in Fig. 3(b) [11,12]. As a result, the $d_{x^2-y^2}$ shell is converted into a doubly occupied electronic ground state [15]. It might lead to a huge orbital moment and strong MCA due to an orbital quantum number of this $d_{x^2-y^2}$ shell higher than that of the d_{z^2} level. Thus, the dominance of both SOC and the trigonal crystal field is responsible for the Ising-like behavior of this spin chain system. On the other hand, the crystallographic trigonal-prism site squeezes with the application of high pressure, resulting in an increase of the crystal-field effect. It ultimately affects the splitting of cobalt d orbitals at the TP site. The d_{z^2} shell lies at a lower energy level while significantly increasing

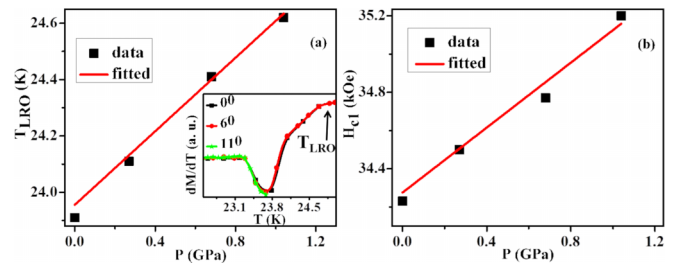


FIG. 4. [(a) and (b)] The hydrostatic-pressure dependence of long-range ordering temperature and critical field of field-driven 3D ferrimagnetic to 3D ferromagnetic transition. The inset of panel (a) shows the plot of the temperature derivative of magnetization vs temperature in different single-crystal orientations at 5 kOe.

the effect of the crystal electric field at high pressure. This would decrease the influence of spin-orbit coupling at higher hydrostatic pressure due to an increase in the tendency of orbital quenching. It reduces the orbital moment contribution to the magnetization and the MCA, correspondingly, in this spin system. In this limit, the Ca₃Co₂O₆ spin system deviates from its Ising-like magnetic nature. Here, a different energy level scheme of crystal-field splitting at the TP site is considered as compared to Ref. [11] to describe the magnetization data at ambient or high pressure, because the d_{z^2} shell is generally the lower energy level in the case of crystal-field splitting at the trigonal prism site as interpreted in Refs. [12,35].

Therefore, the interplay of the crystal-field effect and SOC with applied hydrostatic pressure alter the splitting of d orbitals. This would further modulate the underlying exchange pathways in the CCO system. Some evidence of the exchange interaction modulation of surrounding chains is found in the pressure dependence of T_{LRO} in single-crystalline CCO, which is represented in Fig. 4(a) [6,36–39]. This onset point of long-range ordering is obtained from the first-order derivative of temperature-dependent magnetization with respect to temperature. It depicts a linear variation of T_{LRO} with the application of pressures, and the obtained value of dT_{LRO}/dP is ~ 0.65 K/GPa. It suggests that the coupling strength of the surrounding spin chains is enhanced with the application of high pressure. This strengthening of interchain interaction occurs due to crystal-lattice compression that changes the bond lengths (Co_{TP} -O), the bond angle (Co_{TP} -O-O- Co_{TP}), etc. [40]. The magnetic ordering temperature may depend on the crystal orientation at the low magnetic field as observed in the CrI₃ system [6]. To check whether the T_{LRO} increment [see main panel of Fig. 4(a)] is associated with both the hydrostatic pressure and the single-crystal orientation or the individual effect of external pressure, the orientation dependence of $M(T)$ is carried out after being cooled in the 5-kOe field at ambient pressure. The field-cooled protocol at 5 kOe is followed in this measurement to completely stabilize the ferrimagnetic state at low temperature [28]. The inset shows variation of dM/dT in a small temperature window across T_{LRO} . It indicates that dM/dT data are found to be independent for the given orientations due to a very small magnetization value and its small change with orientation in this narrow temperature range. At the same time, T_{LRO} remains the same in all orientations as shown by the arrow in the inset of Fig. 4(a). It confirms that the enhancement of T_{LRO} as illustrated in the main panel of

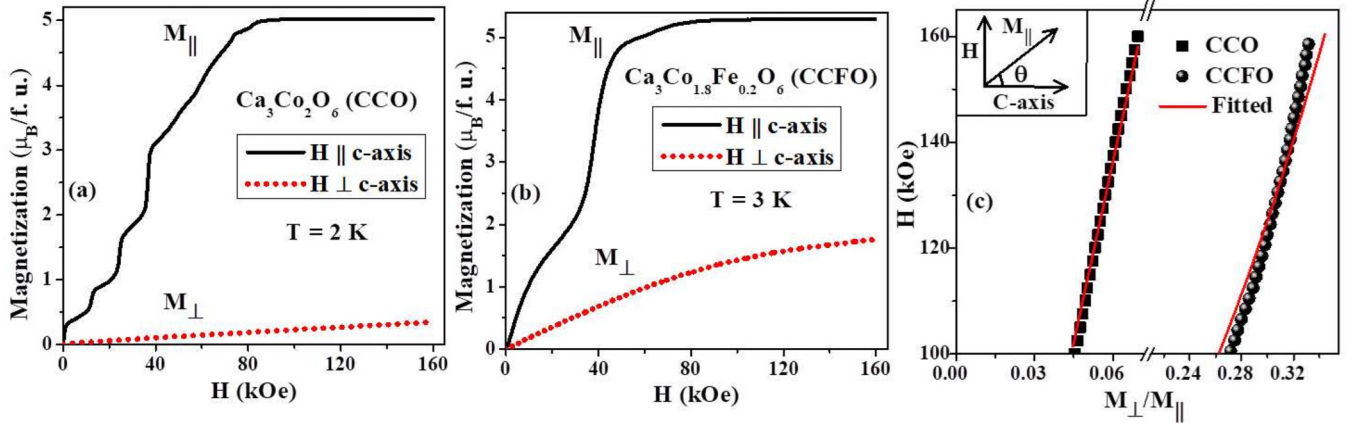


FIG. 5. Panels (a) and (b) illustrate the variation of magnetization as function of magnetic field for parallel (M_{\parallel}) and perpendicular (M_{\perp}) orientation of CCO and CCFO single crystals, respectively. For parallel and perpendicular alignments, the angle between the c axis of the crystals and the applied field are 0° and 90° , respectively, whereas panel (c) and its inset show the plot of the magnetic field vs the ratio of M_{\perp}/M_{\parallel} in the high field range and the schematic diagram of the relative orientation of the magnetization (M_{\parallel}), the applied field (H), and the c axis of the crystal.

Fig. 4(a) is only the manifestation of applied pressures. So, unlike pressure studies in polycrystalline CCO, the effect of a single crystal's orientation can be avoided while applying the pressure in a single crystal by fixing its orientation using the protocol as discussed earlier in this paper [37–39]. Strengthening of interchain coupling is again supported by the pressure dependence of the critical field associated with the 3D FIM to 3D FM transition (H_{c1}), which is a measure of the antiferromagnetic coupling strength of the surrounding chains. This H_{c1} is estimated from the plot of the first-order field derivative of field-dependent magnetization vs projection of the applied field along the crystallographic c axis and its pressure dependence is shown in Fig. 4(b) [23]. Similar to T_{LRO} , it linearly increases with hydrostatic pressures. Moreover, it is also found that $dH_{c1}/dP \sim 0.85$ kOe/GPa, which is completely different as compared to the reported value in the polycrystalline CCO system due to the absence of the single-crystal orientation effect [37–39]. This is further supported by the large orientation dependence of H_{c1} as compared to the pressure dependence of H_{c1} (the data are not included here to avoid confusion). Thus, the modulation in the exchange interaction of the surrounding chains at high pressure arises due to an increase in the crystal-field effect and a decrease in the SOC at high pressure. So, it is obvious that the SOC and trigonal crystal-field effects lead to a huge orbital contribution to the magnetization and the strong MCA in the CCO spin system.

B. Iron-substitution-based studies

1. Classical-model-based calculation of anisotropy constants

Apart from the above qualitative understanding of the MCA in the CCO spin system, a detailed analysis of field-dependent dc magnetization has been performed in CCO and CCFO SCs at ambient pressure to quantitatively explore the MCA. It is expected here that this iron substitution tunes the SOC that finally changes the nature of the MCA due to the quenching of orbitals in $S = 5/2$ iron [41,42]. Figures 5(a) and 5(b) respectively illustrate the variation of

magnetization as a function of the applied field for both parallel and perpendicular orientations of CCO SC at 2 K and CCFO SC at 3 K. In the case of parallel alignment, the magnetization is saturated in both single crystals above 80 kOe. However, the saturation moment is observed to be around $5.3 \mu_B$ in CCFO SC, which is larger than that of the saturation magnetization of the CCO system ($\sim 5.0 \mu_B$). It might be due to the high-spin ($S = 5/2$) state of iron in CCFO, which leads to complete quenching of the orbital moment due to the exactly half-filled d orbital. It is also supported by earlier Mössbauer spectroscopy and magnetization studies in a polycrystalline CCFO compound, which confirms that iron is found to be in high spin and quenched orbital states at both octahedra and prismatic sites [28,43,44]. Hence, iron substitution in the CCO spin system leads to a decrease in the influence of SOC. On the other hand, the observed magnetization value for the perpendicular orientation of both crystals suggests that these systems are far away from the saturation, which is due to the domination of the MCA in these systems. However, the highest magnetization at 160 kOe is increased in the iron-substituted system with respect to the parent compound. It might indicate lessening of the MCA due to the reduced SOC effect in CCFO as compared to that in the CCO spin system. Further, the field-dependent magnetization curves are analyzed using a classical approach to calculate the anisotropy constants and fields in these two systems. It has been applied to pure hexagonal cobalt and other transition metals and many other systems to estimate the anisotropy constants [45,46]. The following procedure is employed here to calculate the important parameters related to the MCA, which is mostly applicable in the high-field range in these systems. The uniaxial anisotropy energy of a crystal can be written as $E_a = K_0 + K_1 \sin^2 \theta + K_2 \sin^4 \theta$, where θ is the angle between the crystallographic c axis and the magnetization parallel to the c axis (M_{\parallel}) as shown in the inset of Fig. 5(c) and K_0 , K_1 , and K_2 are the anisotropy constants [45]. The Zeeman energy of the magnetic field is $E_z = -HM_{\parallel} \cos(90^{\circ} - \theta)$. Thus, the total energy of this crystal, $E = E_a + E_z$, will be minimized for $dE/d\theta = 0$,

TABLE I. The anisotropy constants and fields estimated using the classical model and density functional theory.

Model	Sample	K_1 (meV)	K_2 (meV)	H_a (T)
Classical	$\text{Ca}_3\text{Co}_2\text{O}_6$	32.9	0	227.7
Classical	$\text{Ca}_3\text{Co}_{1.8}\text{Fe}_{0.2}\text{O}_6$	4.06	13.04	196.4
DFT	$\text{Ca}_3\text{Co}_2\text{O}_6$	35.27	1.07	
DFT	$\text{Ca}_3\text{Co}_{1.84}\text{Fe}_{0.16}\text{O}_6$	2.49	6.08	

which gives

$$2K_1 \sin \theta \cos \theta + 4K_2 \sin^3 \theta \cos \theta = HM_{\parallel} \cos(\theta). \quad (1)$$

Moreover, the component of magnetization for perpendicular orientation along the field direction will be

$$M_{\perp} = M_{\parallel} \cos(90^\circ - \theta). \quad (2)$$

Eliminating θ from Eqs. (1) and (2), it can be obtained that

$$H = \frac{2K_1}{M_{\parallel}} \left(\frac{M_{\perp}}{M_{\parallel}} \right) + \frac{4K_2}{M_{\parallel}} \left(\frac{M_{\perp}}{M_{\parallel}} \right)^3. \quad (3)$$

Equation (3) is used to obtain the anisotropy constants in CCO and CCFO systems. The applied field is plotted in Fig. 5(c) vs the magnetization ratio of perpendicular (M_{\perp}) and parallel (M_{\parallel}) directions in the range of 100–160 kOe. A straight line behavior is observed in the CCO system which gives rise to $K_1 = 32.9$ and $K_2 = 0$ meV, respectively, as shown in Table I. This is consistent with an earlier reported value of the anisotropy-related parameter from temperature-dependent susceptibility [10]. It clearly suggests the uniaxial nature of the MCA in this spin system. However, a nonlinear fitted curve appears in the case of fitting with Eq. (3) for the same field range in the CCFO system. It implies that both K_1 and K_2 are found to be nonzero in this system and the obtained values of K_1 and K_2 are 4.06 and 13.04 meV (see Table I), respectively.

The anisotropy constant K_1 is significantly reduced and $K_2 \neq 0$ in CCFO as compared to the CCO system. Therefore, a considerable deviation of the MCA from the uniaxial nature has been found after iron substitution due to lessening of effective SOC. This would discriminate the ideal Ising-like magnetism of the CCO system with respect to the CCFO compound. The weakening of the MCA is also supported by the calculated anisotropy field, $H_a = (2K_1 + 4K_2)/M_{\parallel}$, using

the values of K_1 and K_2 which are listed in Table I for CCO and CCFO single crystals. Hence, the Ising-like nature of the CCO system arises due to SOC and trigonal crystal-field effects.

2. Estimation of anisotropy constants using density functional theory

To gain further insights into the Ising nature of magnetism, the anisotropy constants K_1 and K_2 are estimated using density functional theory (DFT) calculations in $\text{Ca}_3\text{Co}_2\text{O}_6$ and $\text{Ca}_3\text{Co}_{2-x}\text{Fe}_x\text{O}_6$ ($x = 0.16$). The latter designed doped configuration is close to the experimental chemical concentration ($x = 0.2$) and is sufficient enough for understanding the effective change in anisotropy constants as obtained classically. Furthermore, the configuration with Fe at the TP site is found to be lower in energy by 7.52 meV/Co as compared to the configuration wherein the Fe is substituted at the OCT site, consistent with the earlier experimental observations [28]. The DFT calculations are performed with the projector augmented wave (PAW) [47,48] method as implemented in the Vienna *ab initio* simulation package (VASP) [49]. The generalized gradient approximation (GGA) was chosen for the exchange-correlation functional. The effect of strong correlation was incorporated via the effective interaction parameter $U_{\text{eff}} = U - J$ through the rotationally invariant approach of Dudarev *et al.* [50]. In the present study U_{eff} is set to be 5 eV based on the earlier theoretical works on CCO [21]. The Brillouin zone integrations were carried out using $8 \times 8 \times 8$ and $10 \times 10 \times 10$ k-meshes to achieve the self-consistency and to obtain the densities of states (DOS), respectively. The calculations on CCO were performed on the experimentally obtained crystal structure, whereas for CCFO the calculations were performed on the relaxed structure. The atomic positions and volume were relaxed while keeping the space group symmetry intact. The kinetic energy cutoff for the plane-wave basis set was chosen to be 400 eV. The PAW basis functions include $3d$ and $4s$ orbitals for Co and Fe atoms and $2s$ and $2p$ orbitals for O atoms, respectively.

The primary understanding towards the experimentally observed Ising magnetism in CCO with spin degrees of freedom fixed along the \hat{z} direction can be obtained by employing second-order perturbative analysis of the SOC Hamiltonian $H_{\text{SOC}} = \lambda \hat{L} \cdot \hat{S}$. Defining orbital (\hat{L}) and spin (\hat{S}) angular momenta in two independent coordinate systems (x, y, z) and (x', y', z'), the SOC Hamiltonian can be further decoupled as $H_{\text{SOC}} = H_{\text{SOC}}^{\text{sc}} + H_{\text{SOC}}^{\text{snsc}}$, where the expressions for the spin-conserving ($H_{\text{SOC}}^{\text{sc}}$) and spin-nonconserving ($H_{\text{SOC}}^{\text{snsc}}$) terms are given by [51–53]

$$H_{\text{SO}}^{\text{sc}} = \lambda S_z' (L_z \cos \theta + \frac{1}{2} L_+ e^{-i\phi} \sin \theta + \frac{1}{2} L_- e^{i\phi} \sin \theta) = \lambda S_z' (L_z \cos \theta + L_x \sin \theta \cos \phi + L_y \sin \theta \sin \phi) \quad (4)$$

and

$$\begin{aligned} H_{\text{SO}}^{\text{snsc}} &= \frac{\lambda}{2} S_+' (-L_z \sin \theta - L_+ e^{-i\phi} \sin^2 \theta / 2 + L_- e^{i\phi} \cos^2 \theta / 2) + \frac{\lambda}{2} S_-' (-L_z \sin \theta + L_+ e^{-i\phi} \cos^2 \theta / 2 - L_- e^{i\phi} \sin^2 \theta / 2) \\ &= \frac{\lambda}{2} (S_+' + S_-') (-L_z \sin \theta + L_x \cos \theta \cos \phi + L_y \cos \theta \sin \phi). \end{aligned} \quad (5)$$

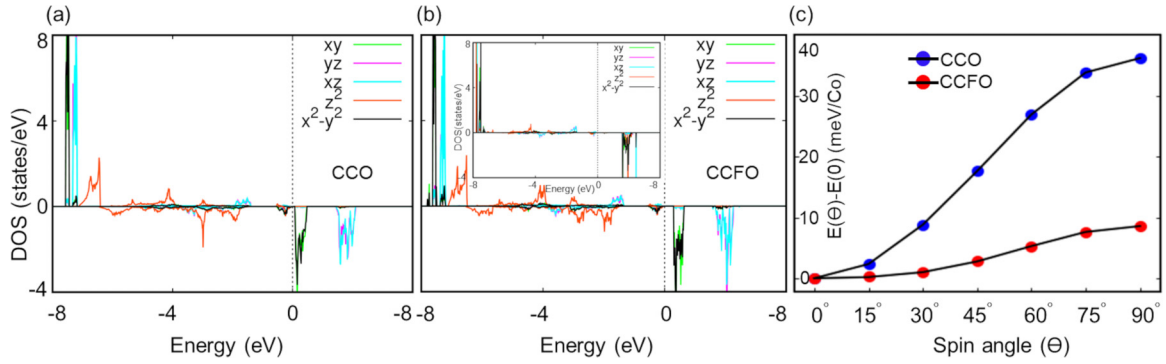


FIG. 6. [(a) and (b)] The spin and orbital resolved density of states calculated within GGA+ U for Co and Fe atoms at the trigonal prismatic site in CCO and CCFO, respectively. The inset of panel (b) depicts the DOS for dopant Fe. Panel (c) shows the variation in the MCA as a function of the polar angle θ for CCO (blue solid circles) and CCFO (red solid circles) and fitted with a function $K_1 \sin^2 \theta + K_2 \sin^4 \theta$ (the black solid line). The calculations were performed by rotating the spin quantization axis within GGA+ U +SOC for $U_{\text{eff}} = 5$ eV.

Here, θ and ϕ are the polar and azimuthal angles, which determine the spin orientation with respect to the (x, y, z) coordinate system. Using perturbation theory, the second-order correction in energy due to H_{SOC} is given by

$$\Delta E_{\text{SOC}} = -\lambda^2 \sum_{\sigma^\sigma, u^{\sigma'}} \frac{|\langle \sigma^\sigma | H_{\text{SOC}} | u^{\sigma'} \rangle|^2}{\epsilon_{\sigma^\sigma} - \epsilon_{u^{\sigma'}}}, \quad (6)$$

where λ is the SOC strength and u^σ (σ^σ) denotes the unoccupied (occupied) states in spin ($\sigma, \sigma' = \uparrow, \downarrow$) channels. The energy difference, $\epsilon_{u^\sigma} - \epsilon_{\sigma^\sigma}$, in the denominator represents the separation between the band centers of unperturbed unoccupied and occupied states. To obtain a qualitative understanding of the MCA from Eq. (6), one needs to examine the energy difference between band centers of the occupied and unoccupied states which are coupled in the same/opposite spin channels and their associated negative/positive contribution to the MCA. The energy difference $\epsilon_{u^\sigma} - \epsilon_{\sigma^\sigma}$ and the related spin coupling are obtained from the spin and orbital resolved DOS shown in Fig. 6(a) within GGA+ U . For CCO, the d manifold is completely occupied in the majority spin-up channel, whereas it is partially occupied in the minority spin-down channel ($z^2 \downarrow$ is occupied), leading to $d^{5\uparrow 1\downarrow}$ ($S = 2$) electronic configuration and hence a Co^{3+} (d^6) charge state consistent with the experimentally observed charge state. Moreover, the $S = 2$ configuration is consistent with the crystal-field splitting of d states in a trigonal prismatic environment. Due to such crystal-field splitting of d states, Eqs. (4) and (5) suggest that the dominant contribution to the MCA will come from the spin-nonconserving term of H_{SO} due to coupling between occupied and unoccupied states in the opposite spin channel, whereas the minor contribution will come from the spin-conserving term due to coupling between states in the same spin channel (the z^2 is the only occupied state in the spin-down channel). Using Eq. (6) and nonvanishing matrix elements of the angular momentum operators: $\langle xz | \hat{L}_z | yz \rangle = 1$, $\langle x^2 - y^2 | \hat{L}_z | xy \rangle = 2$, $\langle z^2 | \hat{L}_x | yz \rangle = \sqrt{3}$, $\langle xy | \hat{L}_x | xz \rangle = 1$, and $\langle x^2 - y^2 | \hat{L}_x | yz \rangle = 1$, the MCA is

estimated to be

$$\begin{aligned} \text{MCA}(\Delta E_{100} - \Delta E_{001}) \\ \sim \lambda^2 \left[\frac{1}{\epsilon_{x^2-y^2\uparrow-xz\downarrow}} + \frac{1}{4\epsilon_{yz\uparrow-xz\downarrow}} - \frac{1}{4\epsilon_{xy\uparrow-xz\downarrow}} \right. \\ \left. - \frac{1}{4\epsilon_{yz\uparrow-x^2-y^2\downarrow}} + \frac{3}{8\epsilon_{z^2\uparrow-yz\downarrow}} \right] > 0, \quad (7) \end{aligned}$$

implying that the easy axis lies along the [001] direction in agreement with the experimental and theoretical studies.

To further quantitatively understand the Ising magnetism and its deviation with Fe doping in CCO, we have estimated the anisotropic constants K_1 and K_2 . These constants are obtained by fitting the energy differences $[E(\theta) - E(0)]$, obtained from the DFT calculations by rotating the spin quantization axis from the [001] direction to the [100] direction ($\phi = 0$) [the blue and red solid circles in Fig. 6(c)], with the parametric equation of the form $K_1 \sin^2 \theta + K_2 \sin^4 \theta$ (solid black line). The results are depicted in Fig. 6(c). The K_1 and K_2 values are found to be 35.27 and 1.07 meV and 2.49 and 6.08 meV for CCO and CCFO, respectively. The anisotropy constants for CCO and the huge reduction in K_1 with Fe doping are in very good agreement with the classically obtained values (see Table I for comparison). However, the absolute values of K_1 and K_2 are varied due to consideration of different iron concentrations in DFT calculations as compared to experiments. We attribute large K_1 values in CCO to the giant orbital moment ($\approx 1.8 \mu_B$) estimated from the DFT+ U +SOC calculation, indicating a pronounced effect of SOC in CCO. However, for CCFO, the orbital moment of Fe gets quenched completely ($\approx 0.01 \mu_B$), which leads to weakening of the MCA and K_1 substantially. To investigate the underlying cause behind the MCA reduction, we have analyzed the spin and orbital resolved DOS of CCFO [see Fig. 6(b)]. The Fe- d manifold is completely occupied in the spin-up channel and is completely empty in the spin-down channel, suggesting that the Fe- d manifold is half-filled. Therefore, as expected, the high-spin ($S = 5/2$) d^5 configuration in a trigonal prismatic crystal-field environment leads to complete quenching of the orbital moment leading to weakening of the MCA.

Hence, the Ising magnetism in CCO and its deviation with Fe doping is in accordance with the experimental observations in this work.

IV. CONCLUSIONS

The Ising-like magnetic nature of $\text{Ca}_3\text{Co}_2\text{O}_6$ spin system is unraveled in this study by tuning the interplay of spin-orbit coupling and crystal-field effects. It is evident that the dominance of spin-orbit coupling and trigonal crystal field is responsible for this Ising-like magnetism. It is proved by considerable weakening of spin-orbit coupling which is respectively achieved by application of high pressure and

Iron substitution. The orbital moment and magnetocrystalline anisotropy are significantly decreased with lessening of this spin-orbit coupling resulting in the deviation from Ising magnetism, which is also substantiated from the density functional theory estimation of anisotropy constants.

ACKNOWLEDGMENTS

We thank Dr. Rajib Rawat and Mr. Kranti Kumar Sharma for fruitful discussions during experiments. B.R.K.N. would like to acknowledge the funding from the Department of Science and Technology, India, through Grant No. CRG/2020/004330.

-
- [1] Y. Tokura and N. Nagaosa, *Science* **288**, 462 (2000).
- [2] M. W. Haverkort, Z. Hu, J. C. Cezar, T. Burnus, H. Hartmann, M. Reuther, C. Zobel, T. Lorenz, A. Tanaka, N. B. Brookes, H. H. Hsieh, H.-J. Lin, C. T. Chen, and L. H. Tjeng, *Phys. Rev. Lett.* **97**, 176405 (2006).
- [3] N. Hollmann, S. Agrestini, Z. Hu, Z. He, M. Schmidt, C.-Y. Kuo, M. Rotter, A. A. Nugroho, V. Sessi, A. Tanaka, N. B. Brookes, and L. H. Tjeng, *Phys. Rev. B* **89**, 201101(R) (2014).
- [4] B. Kim, B. H. Kim, K. Kim, H. C. Choi, S.-Y. Park, Y. H. Jeong, and B. I. Min, *Phys. Rev. B* **85**, 220407(R) (2012).
- [5] S. Son, M. J. Coak, N. Lee, J. Kim, T. Y. Kim, H. Hamidov, H. Cho, C. Liu, D. M. Jarvis, P. A. C. Brown, J. H. Kim, C.-H. Park, D. I. Khomskii, S. S. Saxena, and J.-G. Park, *Phys. Rev. B* **99**, 041402(R) (2019).
- [6] S. Mondal, M. Kannan, M. Das, L. Govindaraj, R. Singha, B. Satpati, S. Arumugam, and P. Mandal, *Phys. Rev. B* **99**, 180407(R) (2019).
- [7] S.-Q. Su, S.-Q. Wu, M. L. Baker, P. Bencok, N. Azuma, Y. Miyazaki, M. Nakano, S. Kang, Y. Shiota, K. Yoshizawa, S. Kanegawa, and O. Sato, *J. Am. Chem. Soc.* **142**, 11434 (2020).
- [8] B. Leedahl, M. Sundermann, A. Amorese, A. Severing, H. Gretarsson, L. Zhang, A. C. Komarek, A. Maignan, M. W. Haverkort, and L. H. Tjeng, *Nat. Commun.* **10**, 5447 (2019).
- [9] H. Kageyama, K. Yoshimura, K. Kosuge, M. Azuma, M. Takano, H. Mitamura, and T. Goto, *J. Phys. Soc. Jpn.* **66**, 3996 (1997).
- [10] V. Hardy, D. Flahaut, R. Frésard, and A. Maignan, *J. Phys.: Condens. Matter* **19**, 145229 (2007).
- [11] H. Wu, M. W. Haverkort, Z. Hu, D. I. Khomskii, and L. H. Tjeng, *Phys. Rev. Lett.* **95**, 186401 (2005).
- [12] Y. Zhang, E. Kan, H. Xiang, A. Villesuzanne, and M.-H. Whangbo, *Inorg. Chem.* **50**, 1758 (2011).
- [13] H. L. Che, J. Shi, J. C. Wu, X. Rao, X. G. Liu, X. Zhao, and X. F. Sun, *AIP Adv.* **8**, 055811 (2018), and references therein.
- [14] S. De and A. Banerjee, *J. Magn. Magn. Mater.* **539**, 168349 (2021); *Physica B* **572**, 125 (2019).
- [15] T. Burnus, Z. Hu, M. W. Haverkort, J. C. Cezar, D. Flahaut, V. Hardy, A. Maignan, N. B. Brookes, A. Tanaka, H. H. Hsieh, H.-J. Lin, C. T. Chen, and L. H. Tjeng, *Phys. Rev. B* **74**, 245111 (2006).
- [16] J.-G. Cheng, J.-S. Zhou, and J. B. Goodenough, *Phys. Rev. B* **79**, 184414 (2009).
- [17] Y. B. Kudasov, A. S. Korshunov, V. N. Pavlov, and D. A. Maslov, *Phys.-Usp.* **55**, 1169 (2012).
- [18] G. Allodi, R. De Renzi, S. Agrestini, C. Mazzoli, and M. R. Lees, *Phys. Rev. B* **83**, 104408 (2011).
- [19] H. Kageyama, K. Yoshimura, K. Kosuge, X. Xu, and S. Kawano, *J. Phys. Soc. Jpn.* **67**, 357 (1998).
- [20] S. Aasland, H. Fjellvåg, and B. Haubackb, *Solid State Commun.* **101**, 187 (1997).
- [21] R. Fresard, C. Laschinger, T. Kopp, and V. Eyert, *Phys. Rev. B* **69**, 140405(R) (2004).
- [22] J. A. M. Paddison, S. Agrestini, M. R. Lees, C. L. Fleck, P. P. Deen, A. L. Goodwin, J. R. Stewart, and O. A. Petrenko, *Phys. Rev. B* **90**, 014411 (2014).
- [23] S. De and A. Banerjee (unpublished).
- [24] S. Agrestini, L. C. Chapon, A. Daoud-Aladine, J. Schefer, A. Gukasov, C. Mazzoli, M. R. Lees, and O. A. Petrenko, *Phys. Rev. Lett.* **101**, 097207 (2008).
- [25] L. C. Chapon, *Phys. Rev. B* **80**, 172405 (2009).
- [26] C. H. Kim, K. H. Kim, S. H. Park, Hyun-jong Paik, J. H. Cho, and B. G. Kim, *J. Phys. Soc. Jpn.* **74**, 2317 (2005).
- [27] S. De, K. Kumar, A. Banerjee, and P. Chaddah, *AIP Conf. Proc.* **1731**, 130026 (2016).
- [28] S. De, V. R. Reddy, and A. Banerjee, [arXiv:2112.13080](https://arxiv.org/abs/2112.13080).
- [29] A. Maignan, C. Michel, A. C. Masset, C. Martin, and B. Raveau, *Eur. Phys. J. B* **15**, 657 (2000).
- [30] V. Hardy, M. R. Lees, O. A. Petrenko, D. Mck. Paul, D. Flahaut, S. Hébert, and A. Maignan, *Phys. Rev. B* **70**, 064424 (2004).
- [31] H. Kageyama, K. Yoshimura, K. Kosuge, H. Mitamura, and T. Goto, *J. Phys. Soc. Jpn.* **66**, 1607 (1997).
- [32] C. Zobel, M. Kriener, D. Bruns, J. Baier, M. Grüninger, T. Lorenz, P. Reutler, and A. Revcolevschi, *Phys. Rev. B* **66**, 020402(R) (2002).
- [33] J. B. Goodenough, *J. Phys. Chem. Solids* **6**, 287 (1958).
- [34] J. A. Real, A. B. Gaspar, and M. C. Muñoz, *Dalton Trans.* **12**, 2062 (2005).
- [35] R. Huisman, R. D. Jonge, C. Haas, and F. Jellinek, *J. Solid State Chem.* **3**, 56 (1971); R. L. Carlin and A. J. van Duyneveldt, *Magnetic Properties of Transition-Metal Compounds* (Springer-Verlag, Berlin, 1977).
- [36] Y. Sun, R. C. Xiao, G. T. Lin, R. R. Zhang, L. S. Ling, Z. W. Ma, X. Luo, W. J. Lu, Y. P. Sun, and Z. G. Sheng, *Appl. Phys. Lett.* **112**, 072409 (2018).
- [37] B. Martínez, V. Laukhin, M. Hernando, J. Fontcuberta, M. Parras, and J. M. González-Calbet, *Phys. Rev. B* **64**, 012417 (2001).

- [38] T. Goko, N. Nomura, S. Takeshita, and J. Arai, *J. Magn. Magn. Mater.* **272-276**, E633 (2004).
- [39] M. Hernando, B. Martínez, V. Laukhin, J. Fontcuberta, M. Parras, and J. M. González-Calbet, *J. Magn. Magn. Mater.* **242-245**, 757 (2002).
- [40] D. P. Kozlenko, N. T. Dang, N. O. Golosova, S. E. Kichanov, E. V. Lukin, P. J. Lampen Kelley, E. M. Clements, K. V. Glazyrin, S. H. Jabarov, T. L. Phan, B. N. Savenko, H. Srikanth, and M. H. Phan, *Phys. Rev. B* **98**, 134435 (2018).
- [41] J. Arai, H. Shinmen, S. Takeshita, and T. Goko, *J. Magn. Magn. Mater.* **272-276**, 809 (2004).
- [42] M. A. McGuire, K. V. Shanavas, M. S. Kesler and D. S. Parker, *Sci. Rep.* **8**, 14206 (2018).
- [43] H. Kageyama, S. Kawasaki, K. Mibu, M. Takano, K. Yoshimura, and K. Kosuge, *Phys. Rev. Lett.* **79**, 3258 (1997).
- [44] I. Nowik, A. Jain, S. M. Yusuf, and J. V. Yakhmi, *Phys. Rev. B* **77**, 054403 (2008); A. Jain, S. Singh, and S. M. Yusuf, *ibid.* **74**, 174419 (2006).
- [45] B. D. Cullity and C. D. Graham, *Introduction to Magnetic Materials*, 2nd ed. (Wiley & Sons, Hoboken, NJ, 2008), p. 221.
- [46] F. Ono, *J. Phys. Soc. Jpn.* **50**, 2564 (1981); S. Sharma, E. Hildebrandt, M. Major, P. Komissinskiy, I. Radulov, and L. Alff, *J. Magn. Magn. Mater.* **452**, 80 (2018).
- [47] G. Kresse and D. Joubert, *Phys. Rev. B* **59**, 1758 (1999).
- [48] P. E. Blöchl, *Phys. Rev. B* **50**, 17953 (1994).
- [49] G. Kresse and J. Furthmüller, *Phys. Rev. B* **54**, 11169 (1996).
- [50] S. L. Dudarev, G. A. Botton, S. Y. Savrasov, C. J. Humphreys, and A. P. J. Sutton, *Phys. Rev. B* **57**, 1505 (1998).
- [51] X. Wang, R. Wu, D.-S. Wang, and A. J. Freeman, *Phys. Rev. B* **54**, 61 (1996).
- [52] D.-s. Wang, R. Wu, and A. J. Freeman, *Phys. Rev. B* **47**, 14932 (1993).
- [53] A. Chauhan and B. R. K. Nanda, *Appl. Phys. Lett.* **119**, 261906 (2021).